

THE LHC VACUUM SYSTEM

Oswald Gröbner, for the LHC Vacuum Group
CERN, Geneva, Switzerland

Abstract

The Large Hadron Collider (LHC) project, now in the advanced construction phase at CERN, comprises two proton storage rings with colliding beams of 7-TeV energy. The machine is housed in the existing LEP tunnel with a circumference of 26.7 km and requires a bending magnetic field of 8.4 T with 14-m long superconducting magnets. The beam vacuum chambers comprise the inner 'cold bore' walls of the magnets. These magnets operate at 1.9 K, and thus serve as very good cryo-pumps. In order to reduce the cryogenic power consumption, both the heat load from synchrotron radiation emitted by the proton beams and the resistive power dissipation by the beam image currents have to be absorbed on a 'beam screen', which operates between 5 and 20 K and is inserted inside the vacuum chamber. The design of this beam screen represents a technological challenge in view of the numerous and often conflicting requirements and the very tight mechanical tolerances imposed. The synchrotron radiation produces strong outgassing from the walls. The design pressure necessary for operation must provide a beam lifetime of several days. An additional stringent requirement comes from the power deposition in the superconducting magnet coils due to protons scattered on the residual gas, which could lead to a magnet, quench and interrupt the machine operation. Cryopumping of gas on the cold surfaces provides the necessary low gas densities but it must be ensured that the vapour pressure of cryosorbed molecules, of which H_2 and He are the most critical species, remains within acceptable limits. In the warm straight sections of the LHC the pumping speed requirement is determined by ion-induced desorption and the resulting vacuum stability criterion.

1. INTRODUCTION

The Large Hadron Collider (LHC) [1] consists of a pair of superconducting storage rings with a circumference of 26.7 km. Two proton beams, of 530 mA and an energy of 7.0 TeV, circulate in opposite directions. Of the 54-km total length, the arcs account for almost 48 km and will be at 1.9 K, the temperature of the superconducting magnets. The basic layout of LHC follows the existing LEP machine, with eight long straight sections and eight bending arcs. The present experimental programme includes two high-luminosity experiments (ATLAS and CMS) as well as a heavy ion experiment (ALICE) and a B-physics experiment shown schematically in Fig.1. In this figure is also shown the position for the two beam transfer lines from the existing SPS accelerator, which will be used as the injector, the locations for the accelerating RF system, the beam dump system and the two beam cleaning insertions.

To fit the 7-TeV rings into the existing LEP tunnel special design concepts are needed for the machine components and, most specifically, superconducting magnets with 8.3 T field. The magnetic bending field of 8.3 T implies that the superconducting magnets which use commercially available NbTi superconductors must operate at a temperature well below 4.2 K. A very attractive technical solution for the LHC has been to immerse the magnets in a bath of superfluid helium at 1.9 K. A selection of the most significant machine parameters is given in Table 1.

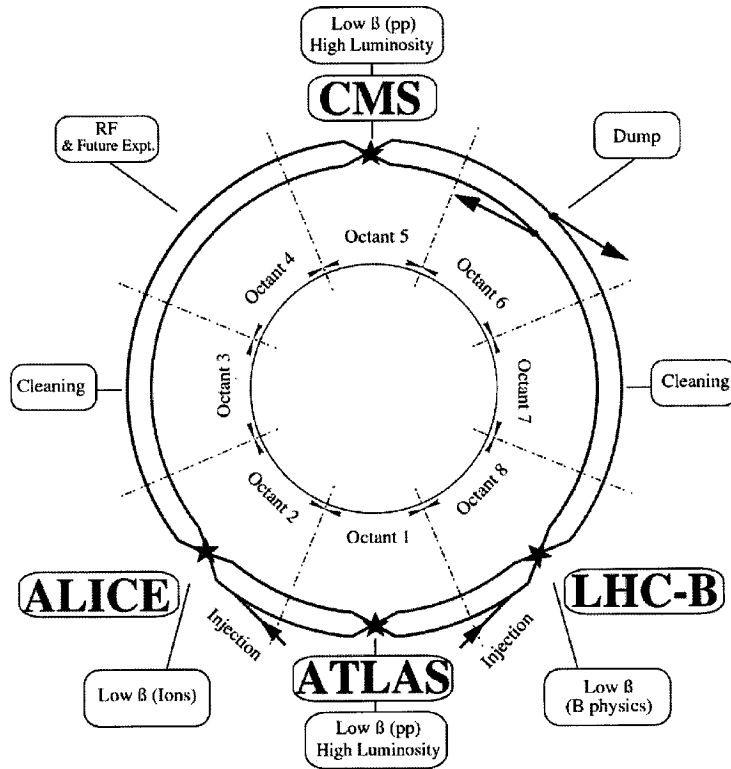


Fig. 1 General layout of LHC

Table 1
Principal machine parameters for proton-proton collisions

	Value	Unit
Energy	7	TeV
Dipole field	8.33	T
Coil aperture	56	mm
Luminosity	10^{34}	$s^{-1} cm^{-2}$
Injection energy	450	GeV
Circulating current /beam	0.56	A
Bunch spacing	25	ns
Particles/bunch	$1.1 \cdot 10^{11}$	
Stored beam energy	350	MJ
Normalised transverse emittance	3.75	μm
R.m.s. bunch length	0.075	m
Beam lifetime	22	h
Luminosity lifetime	10	h
Energy loss/turn	6.7	keV
Critical photon energy	45	eV
Linear photon flux	$1 \cdot 10^{17}$	$m^{-1} s^{-1}$
Total radiated power/beam	3.8	kW

The magnets for LHC are based on a two-in-one design, where the two beam channels are incorporated into a common iron yoke in a compact single cryostat [2]. Figure 2 illustrates this design concept showing the cross section of a dipole magnet with its cryostat. A similar design has been adopted for the quadrupole magnets of the short straight sections (sss). The compact machine design which results from this construction allows the installation of the LHC machine inside the existing tunnel section of LEP and makes the necessary provision for the addition of a LEP-like machine on top of LHC at some later time.

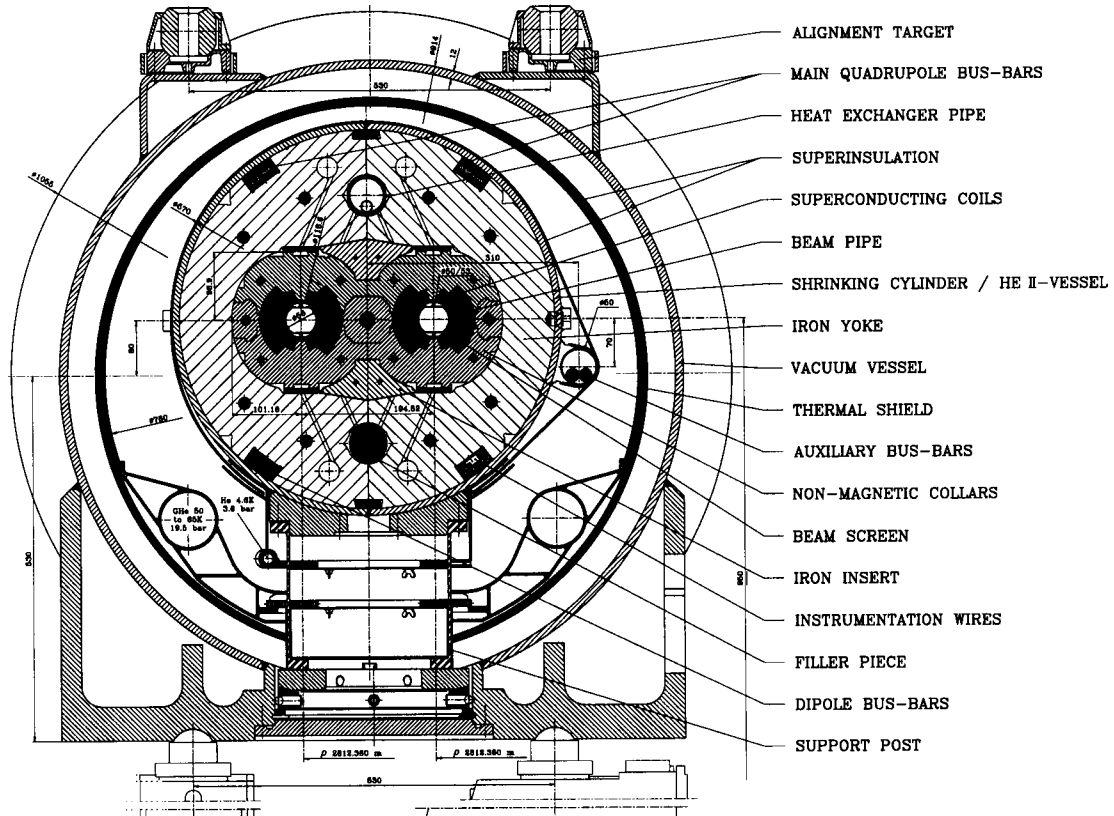


Fig. 2 Dipole magnet cross section with cryostat

In the arcs of LHC, representing more than 24 km of each ring, the machine lattice consists of a succession of regular 53.4-m long 'half-cells': three 14.2-m long twin-aperture dipole magnets, and one 6.3-m long short straight section. The remaining space is taken by various machine elements and by interconnections between magnets. In the eight long straight sections the machine layout is adapted to the specific requirements of the experiments or of the other functions and the repetitive, regular design is locally modified. In the four experimental straight sections, the beams converge into one common beam pipe, where they are tightly focused and steered into head-on collisions at the interaction points.

2. THE VACUUM SYSTEM

The vacuum system for LHC consists of two main parts which are kept entirely separated in terms of vacuum since they must meet rather different requirements: the cryogenic insulation vacuum necessary to avoid heat load by gas conduction requires a pressure of only about 10^{-6} mbar while the beam vacuum proper which must provide a good beam lifetime and low background for the experiments requires several orders of magnitude better vacuum for the operation with beam.

2.1 Cryogenic insulation vacuum

The cryogenic insulation vacuum for the machine consists of a nearly 3-km long continuous arc cryostat, which is, subdivided into 14 sectors each 212-m long [3]. Vacuum separation is achieved by

vacuum barriers which subdivide the arc cryostat into subsections which can be pumped, commissioned and leak checked independently. These vacuum barriers also separate the vacuum for the continuous cryogenic distribution line (QRL) from the machine cryostat as shown in Fig. 3.

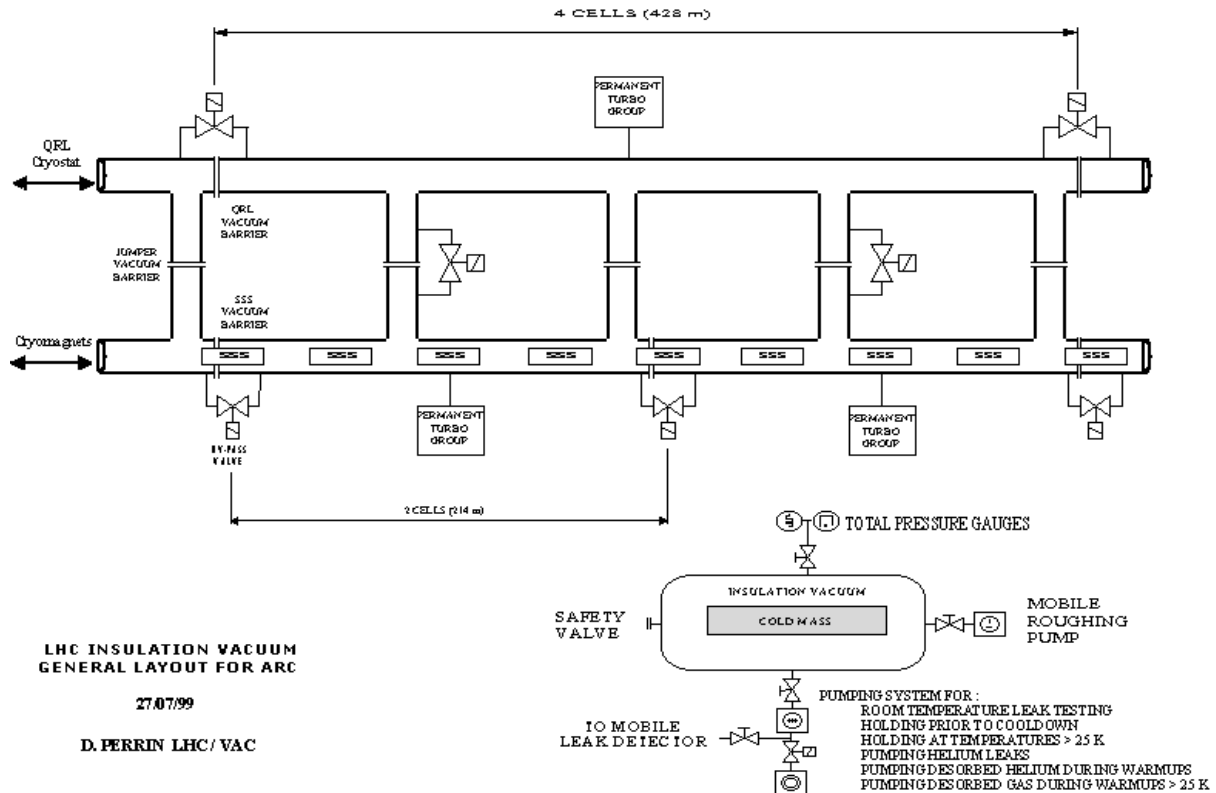


Fig. 3 Layout of cryogenic insulation vacuum

While the initial pump down can be done with conventional turbomolecular pumping groups shown in the insert of the Fig. 3, the cryopumping on the large external surface of the magnet cold mass and on the thermal screens will be entirely sufficient for maintaining the static insulation vacuum once the system has been cooled down. Provisions for any additional pumping during machine operation are required only in the case that excessive helium leaks would occur. This additional pumping can be achieved either by connecting external pumps or by installing charcoal-coated cryo-panels with a large pumping capacity for helium. Whether this option is actually needed to recover from a degraded vacuum remains to be decided on the basis of a failure analysis and based on experience with the final installation procedure and a test string of the machine.

2.2 Beam vacuum and beam related heat loads

The beam vacuum system has been the subject of extensive studies over the recent years and has been presented at several occasions [4–6]. The beam pipe in the centre of the superconducting magnet coils, as illustrated in Fig. , is in direct contact with the helium bath at 1.9 K (cold-bore beam pipe) so as to minimise the loss of aperture between the magnet coils and the beam stay-clear region.

At this temperature, the vacuum chamber wall becomes a very efficient cryopump with practically infinite capacity for all condensable gas species with the sole exception of helium and thus makes any external pumping superfluous and even inefficient. Unfortunately, this concept has the drawback that the cryogenic system will have to remove even very small amounts of beam induced power which, for conventional room temperature accelerators, would be insignificant. Indeed, since the removal of 1 W at 1.9 K requires nearly 1 kW of electric power, there is a strong incentive to avoid or to reduce to the bare minimum any source of heat in-leak to the cold beam pipe.

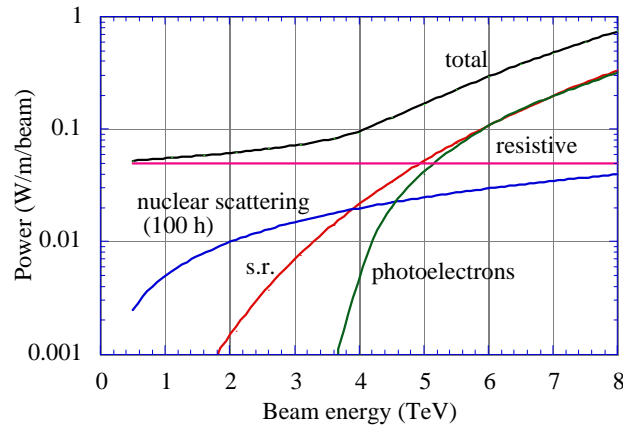


Fig. 4 Beam-induced losses in the LHC

Four distinct beam and vacuum related heat sources to the 1.9 K system can be identified as shown in Fig. 4 and these will be discussed in more detail in the following sections:

i) Synchrotron radiation

Due to the centripetal acceleration in the bending magnets the beams will emit a synchrotron radiation flux of about 10^{17} photons $s^{-1} m^{-1}$ with a critical energy of the photon spectrum of 45 eV equivalent to a distributed linear power of $0.2 W m^{-1}$. For LHC as a whole, this amounts to 7.6 kW.

ii) Image currents from the beam

The inner wall of the beam pipe must conduct the image currents of the beams, which may dissipate typically $0.05 W m^{-1}$ per beam duct. This power due to image currents depends directly on the resistivity ρ_w of the vacuum chamber wall material. To limit this heat load, but also to avoid resistive wall instability, the resistivity of the vacuum chamber has to be low. For the LHC this can be achieved by coating the inner surface of the stainless steel beam pipe with a thin copper layer and by profiting, furthermore, from the fact that at low temperature the resistivity of high-purity copper is strongly reduced and can be by a factor of 10^3 better than for stainless steel.

iii) Photo-electrons and multipacting

Beam induced multipacting can arise through an oscillatory motion of a cloud of photo-electrons and of low energy secondary electrons bouncing back and forth between opposite vacuum chamber walls during successive passages of proton bunches [7]. Due to the strong electric field of the dense proton beam these electrons will be accelerated and transfer their energy to the cold wall. In the LHC the beam pipe radius r_p , the bunch intensity N_b and the bunch spacing L_{bb} are such that the wall-to-wall multipacting threshold corresponds to about 1/4 of the nominal intensity [8]. The magnitude of the heat load depends on several parameters as will be discussed in a later section but a crude estimate indicates a value of $0.2 W/m$.

iv) Beam loss by nuclear scattering

Nuclear scattering of the high-energy protons on the residual gas generates an unavoidable continuous flux of high-energy particles, which are lost from the circulating beams. Even under ideal conditions there remains a small fraction of scattered protons which can not be absorbed in a controlled way by the dedicated set of collimators in the beam cleaning insertions (see Fig. 1). These particles escape from the aperture of the machine and penetrate through the cold bore into the magnets where they are lost. This flux of high-energy protons creates a shower of secondary particles, which are ultimately absorbed in the 1.9 K magnet system. The continuous heat input to the cryogenic system is directly proportional to the gas density and hence the maximum allowed value defines an upper limit of the gas density in the beam pipe. The beam lifetime τ , due to nuclear scattering (the cross section for 7-TeV protons on hydrogen atoms is $\sigma \sim 5 \cdot 10^{-30} m^2$) is given by

$$\frac{1}{\tau} = c\sigma n \quad (1)$$

where c is the speed of light and n the gas density. The linear power load, P (W/m), is proportional to the beam current I , the beam energy E and can be expressed directly in terms of the beam-gas lifetime

$$P = \frac{IE}{c\tau} = 0.93 \frac{E(\text{TeV})I(\text{A})}{\tau(\text{h})} \quad (2)$$

For the first time in an accelerator, beam loss due to nuclear scattering on the residual gas represents a non-negligible heat load. The machine design includes therefore a nuclear scattering allowance of ~ 0.1 W/m for the two beams. Consistent with this requirement a beam lifetime of ~ 100 hours has been chosen which in turn implies that the H_2 density must be $\leq 1 \times 10^{15}$ molecules m^{-3} (e.g. equivalent to a pressure of $\leq 1 \times 10^{-9}$ Torr at 10 K). A correspondingly lower density is required for heavier gases as is shown in Table 2 where the limits of the molecular densities for some common gas species have been listed.

Table 2
Relative cross sections and maximum gas densities for different gas species

Gas	S/s _{H₂}	N (m ⁻³) for $\tau = 100$ h
H ₂	1	1 10 ¹⁵
He	1.26	7.8 10 ¹⁴
CH ₄	5.4	1.8 10 ¹⁴
H ₂ O	5.4	1.8 10 ¹⁴
CO	7.8	1.2 10 ¹⁴
CO ₂	12.2	8.0 10 ¹³

Among the four heat sources shown in Fig. 4 synchrotron radiation, image currents and photo-electrons can be intercepted at a thermodynamically-more-efficient temperature of 20 K. This can be achieved by inserting in the cold bore vacuum chamber a thermally insulated ‘beam screen’, which is actively cooled by gaseous helium. The fourth component, due to scattered high-energy protons, cannot be intercepted by this screen and must be included in the cryogenic budget for the 1.9 K system. This effect, which has a practical importance for the first time in the LHC, defines a ‘lifetime limit’ of 10^{15} H₂ molecules m^{-3} for the maximum average gas density in the LHC arcs. It must be noted that in the exceptional case of a limited region with a very high pressure, e.g. for a helium leak, the related beam loss may even trigger a magnet to quench.

The section of the beam screen with its two cooling tubes is shown in Fig. 5. In order not to lose the benefit of the cryopumping on the 1.9 K cold bore, the screen has narrow pumping slots along its length which enable gas molecules to leave the beam channel proper and to be adsorbed on the cold bore wall. The importance of cryosorbing gas molecules on a surface, which is screened from the effects of the beam, will be discussed in the following section.

3. PRIMARY DESORPTION BY SYNCHROTRON RADIATION

At 7 TeV, the critical energy of the synchrotron radiation spectrum is ~ 45 eV and the radiated power represents a heat load of 0.2 W/m per beam. The actively-cooled beam screen intercepts this power so that it does not load the 1.9 K system. For vacuum reasons, the screen has to be partially transparent so that molecules desorbed by the synchrotron radiation can escape from the beam channel and be pumped permanently on the cold bore surface as illustrated in Fig. 5.

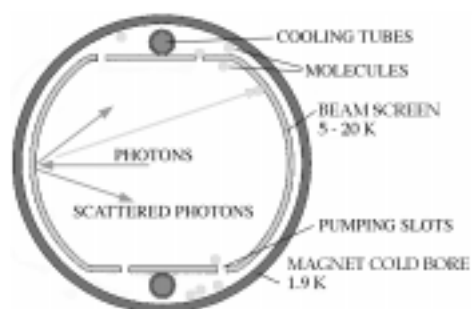


Fig. 5 Actively-cooled beam screen in the magnet cold bore

The synchrotron radiation, which strikes the copper-coated inner surface, liberates a significant amount of gas, proportional to the photon flux and to the molecular desorption yield. The molecular yield for H_2 from a copper surface at 10 K is typically $5 \cdot 10^{-4}$ molecules per photon while other species have considerably smaller values. Figure 6 shows the primary molecular desorption yield for copper-coated stainless steel as a function of the photon dose measured on a test chamber at 77 K, grazing photon incidence and with a critical photon energy of 50 eV.

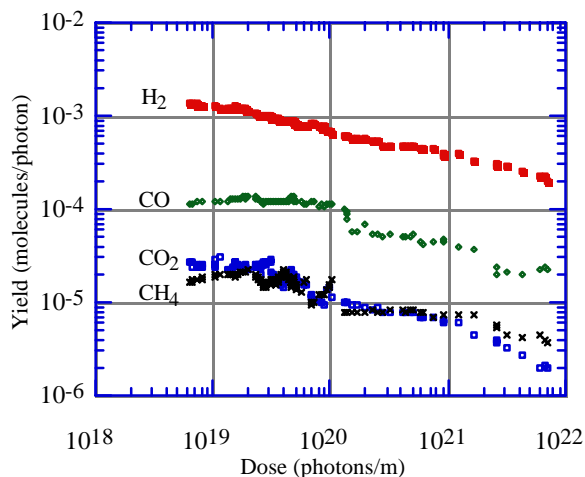


Fig. 6 Primary molecular-desorption yield versus accumulated photon dose

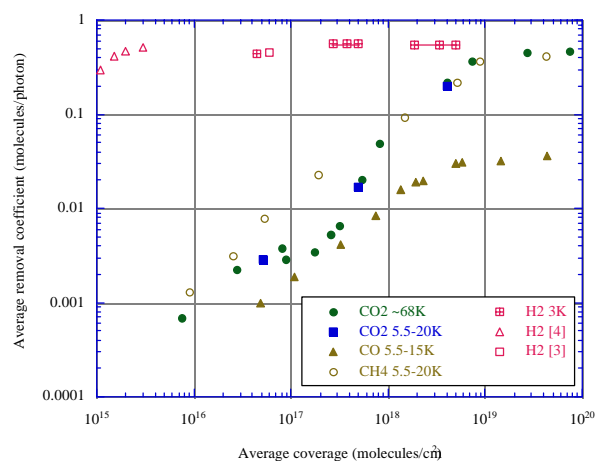


Fig. 7 Re-cycling coefficient for different gas species as a function of the coverage

4. VAPOUR PRESSURE AND RECYCLING OF PHYSORBED GAS

Among the desorbed molecules, hydrogen, which has the largest molecular desorption yield, is the most critical species for which the thermal desorption is high and the sorption capacity at the temperature of the beam screen surface is rather small. Without the pumping holes, the surface of the screen would therefore not provide any useful pumping capacity since the equilibrium vapour density at 5 K for a monolayer of hydrogen exceeds by several orders of magnitude the acceptable limit [9]. With the concept of pumping holes however, hydrogen, and even more so all other gas species, will be crysorbed on the 1.9 K surface with a negligibly-low vapour pressure and hence with a practically unlimited capacity.

Since direct and scattered/reflected photons as well as photo-electrons continuously strike the interior surface of the beam screen, crysorbed gas molecules are efficiently re-desorbed. This 'recycling' effect increases with surface coverage and may dominate other sources of outgassing. The global result of thermal desorption and of recycling of gas implies that only a small quantity of gas can be accommodated on the inner surface of the beam screen. Thereafter any additional molecules will gradually escape through the holes and the pressure rise stabilises when the rate of production of gas molecules equals the pumping through the holes.

Experimental data for the recycling effect have been obtained from an experiment at the VEPP-2M storage ring at the Budker Institute of Nuclear Physics (BINP) in Novosibirsk, Russia [10]. In this experiment a sample can be loaded initially with a known quantity of a gas. Subsequently, the sample is exposed to a known number of photons and the quantity of molecules remaining after this exposure is measured during its warm-up. The results of this experiment are given in Fig. 7 where it can be seen that the recycling of H_2 by synchrotron radiation photons is a very pronounced effect already at a coverage well below a monolayer ($< 10^{15}$ molecules cm^{-2}).

It is interesting to note that this recent result for the hydrogen re-cycling coefficient is in good agreement with observations made previously when investigating the problem of an abnormal hydrogen vapour pressure in condensation cryopumps [11]. It was observed that exposure to room temperature thermal radiation can desorb very strongly hydrogen condensed on a substrate at 2.3 K. Indeed, extrapolating from these earlier measurements to LHC conditions, the synchrotron radiation power density on a cold bore without screen (~ 0.14 W cm^{-2}) could increase the saturated vapour pressure to a value comparable to the lifetime limit.

The evolution of the vacuum pressure is illustrated in Fig. 8 which shows the experimental results from a test at the VEPP-2M photon beam line at BINP [12]. For better comparison, the data shown in the figure have been scaled to the photon flux in the LHC corresponding to the initial conditions of 1/10 of the nominal current. With a $\sim 2\%$ area of pumping holes, hydrogen saturates at $\sim 3 \cdot 10^{13}$ m^{-3} , which is well below the specified lifetime limit. Warming the beam screen to 77 K while maintaining the cold-bore at ~ 3 K, to the remove cryosorbed hydrogen demonstrates the recycling effect of cryosorbed gas on the inner wall of the beam screen. This process effectively desorbs all the hydrogen. During the second exposure hydrogen accumulates again on the screen until the gas density reaches a new saturation level.

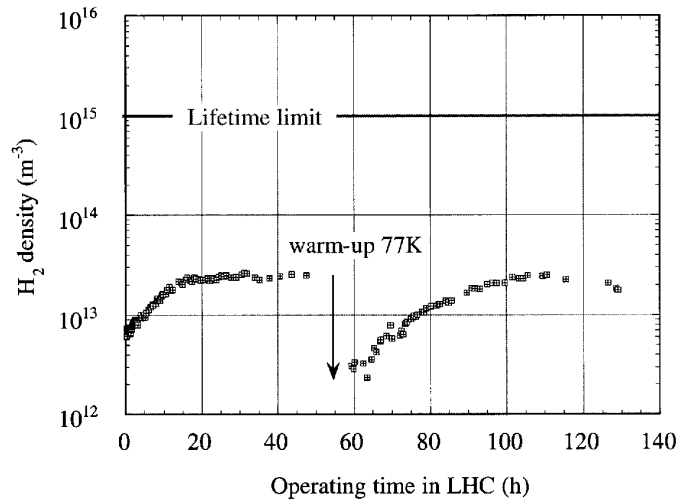


Fig. 8 Evolution of the hydrogen density during photon exposure

5. DYNAMIC MODEL FOR H_2

The dynamic vacuum behaviour for hydrogen in the cold parts of LHC with a perforated beam screen may be described very accurately by a linear model for the interaction between the volume density, n (m^{-3}), and the surface density, Θ (m^{-2}), of adsorbed molecules on the wall of the beam screen. The volume and the surface gas interact according to the following set of linear equations:

$$V \frac{dn}{dt} = q - an + b\Theta \quad (3)$$

and

$$F \frac{d\Theta}{dt} = c n - b \Theta . \quad (4)$$

Here, V is the volume and F is the net wall area per unit length of the vacuum system. The parameters a , b , c and q represent the following physical quantities:

i) q represents a source of gas, here in particular the photon induced desorption rate determined by the product of the desorption yield, η (molecules/photon), and of the photon flux, $\dot{\Gamma}$, hence $q = \eta \dot{\Gamma}$ (molecules $s^{-1}m^{-1}$). In more general terms q can include any source of chemisorbed gas e.g. by ion- or by electron-stimulated desorption.

ii) a ($m^2 s^{-1}$) describes the total pumping on the surface of the wall and in particular through the area of the holes in the beam screen. It can be expressed as

$$a = \frac{1}{4} \bar{v} F (s + f) \quad (5)$$

where \bar{v} is the average molecular velocity, s the sticking probability of the molecules on the beam screen and f is the fraction of the total surface of the beam screen with pumping holes, note that $f \ll 1$.

iii) b represents gas originating from a physisorbed surface phase, Θ , by thermal- and by photon-induced desorption. In contrast to q , this is not a source of 'new' gas but constitutes a surface phase interacting through adsorption and desorption with the gas in the volume.

The thermal contribution to b [13] may be expressed as the molecular vibration frequency $\nu_0 = 10^{13} s^{-1}$ multiplied with a Boltzmann factor

$$e^{-E/kT} \quad (6)$$

characterised by its activation energy E and by the temperature T .

The photon-induced desorption process can be expressed as $\kappa \dot{\Gamma}$, where κ is the re-cycling cross-section in m^2 per photon, thus

$$b = F \nu_0 e^{-E/kT} + \kappa \dot{\Gamma} . \quad (7)$$

iv) c is the rate of adsorption of gas molecules on the surface of the beam screen only. This effect is proportional to the sticking probability of the molecules, s ,

$$c = \frac{1}{4} \bar{v} s F . \quad (8)$$

This dynamic model contains a reasonably small number of parameters, which, for simplicity may be assumed to be constant. In particular it implies a linear adsorption isotherm.

$$\Theta = \frac{c}{b} n = \frac{\frac{1}{4} \bar{v} s F}{F \nu_0 e^{-E/kT} + \kappa \dot{\Gamma}} n . \quad (9)$$

Here Θ (n) depends on the re-cycling cross-section as well as on the photon flux. Therefore, the isotherm and the equilibrium surface coverage for a given volume gas density will depend on these specific conditions (i.e. on the beam current) which effectively reduce the sojourn time of any physisorbed molecules on the surface.

As shown in Fig. 9 the experimental data presented in Fig. 8, can indeed be described in a very satisfactory manner by this simple model by choosing a small number of free parameters only, see Table 3. Parameters shown in bold face have been adapted to best fit the data. The fraction of pumping slots f , takes into account the Clausing factor due to the wall thickness of the beam screen.

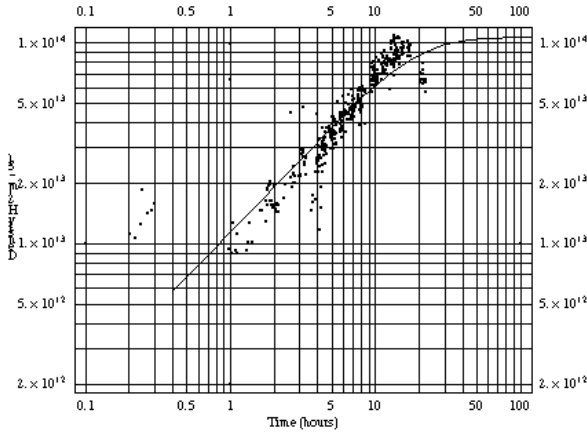


Fig. 9 Comparison of experimental data with the dynamic model for H_2 density (m^{-3}) as a function of time

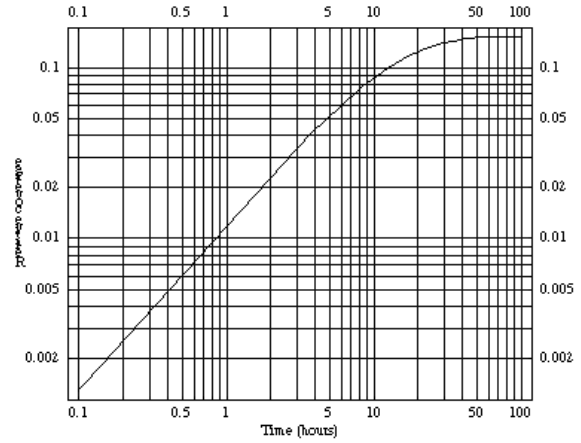


Fig. 10 Surface density of H_2 molecules normalised to a monolayer coverage as a function of time

Table 3
List of parameters.

Desorption yield	η	5×10^{-4} molecules/photon
Screen temperature	T	10 K
Linear photon flux (200 mA)	$\dot{\Gamma}$	3.14×10^{16} photons/s/m
Sticking probability	σ	0.6
Monolayer capacity		3×10^{19} molecules/ m^2
Re-cycling coefficient	κ	$5 \times 10^{-21} m^2$
Activation energy	E	800 cal/mole or 0.035 eV/molecule
Specific surface area	F	0.14 m
Fraction of pumping slots	f	1.28%
Specific volume	V	$1.3 \times 10^{-3} m^2$

The model provides in addition to the volume density also the surface density of gas, which is shown in Fig. 10. There it can be observed that the final coverage obtained remains indeed well below a monolayer as a result of the strong recycling of gas molecules.

In equilibrium conditions, when the volume and surface densities no longer change with time, the volume density is simply given by

$$n_{equ} = \frac{q}{a - c} = \frac{\eta \dot{\Gamma}}{\frac{1}{4} \bar{v} F f} \quad (10)$$

and depends solely on the primary desorption by synchrotron radiation and on the pumping through the holes in the beam screen.

6. ION STIMULATED DESORPTION AND PRESSURE INSTABILITY

Ionization of the residual gas molecules will produce ions, which are ejected by the positive beam potential and accelerated towards the beam screen. The final impact energy of the ions may be up to 300 eV in the arcs of the LHC. As with photons, the energetic ions are very effective in desorbing tightly-bound gas molecules, a process, which is characterised by the molecular, desorption yield, η_i (molecules per ion). Desorbed molecules may in turn be ionised and thus increase the desorption rate. This positive feedback can lead to the so-called ‘ion-induced pressure instability’ known from previous experience with the Intersecting Storage Rings (ISR) at CERN [14]. As a result of this feedback mechanism the pressure increases with beam current from the initial value, P_0 , as

$$P_I = \frac{P_0}{1 - \frac{\eta I}{(\eta I)_{crit}}} . \quad (11)$$

Since the electric charge of the beam is strongly concentrated in 2835 individual, short bunches, the resulting instantaneous peak electric field amounts to several kV. The final energy of the ions at the impact on the vacuum chamber wall can reach several hundred eV depending on the beam intensity and the type of ion. Fig. 11 shows the impact energies calculated for H_2 , He, CH_4 , CO and CO_2 ions as a function of the average beam intensity. Because of the bunched structure of the beam, light ions may gain considerably more energy than heavier ones.

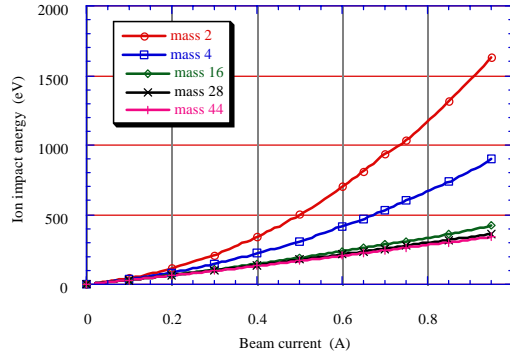


Fig. 11 Ion impact energy as a function of beam current

The pressure runaway depends critically on the local cleanliness of the surface, through the ion-induced molecular desorption yield, η_i , and on the local pumping speed. The stability limit is expressed by the condition that the product of beam current I and of the molecular desorption yield must be less than a critical value given by the effective pumping speed of the system, S_{eff}

$$(\eta_i I)_{crit} = \frac{e}{\sigma} S_{eff} \quad (12)$$

where e is the electron charge and σ the ionisation cross section of the residual gas molecules for high energy protons. According to Eq. (12) the pressure will double at half the critical value. Ionisation cross sections for high energy protons for some common gas molecules are given in Table 4 [15].

Table 4
Ionisation cross sections for some common molecules

Gas	Ionization cross-section (in 10^{-18} cm^2)	
	26 GeV	7000 GeV
H ₂	0.22	0.37
He	0.23	0.38
CH ₄	1.2	2.1
CO	1.0	1.8
Ar	1.1	2.0
CO ₂	1.6	2.8

The effective pumping speed in the cold sections of the LHC can be very large for molecules, which condense on the wall of the beam screen. However, it has a well defined, lower limit determined by the cryosorption on the 1.9 K vacuum chamber surface through the pumping holes in the beam screen. The condition for vacuum stability can be defined by the area f of pumping holes per unit length

$$(\eta_i I)_{crit} = \frac{1}{4} \frac{e}{\sigma} \bar{v} f . \quad (13)$$

From this equation the stability limit for the cold arc is typically 10^3 A for hydrogen and somewhat less for the other gas species. The gradual accumulation of physisorbed gas on the wall leads to an increasing desorption yield which may reach values as large as 10^3 H₂ molecules/ion at a monolayer [16]. Nevertheless, with the high effective pumping speed of the holes the cold sections with beam screens are expected to operate well inside this stability limit. In addition, as shown in Fig. 10, the equilibrium surface coverage for H₂ will not increase indefinitely but should remain well below a monolayer due to the continuous re-cycling effect and the pumping through the holes. Therefore, the ion-induced pressure instability can be avoided by ensuring that molecules are cryosorbed on surfaces, which are in the shadow of the beam.

More serious is the vacuum stability in the warm sections of LHC due to the limited pumping speed, which can be provided by conventional pumps, and the limited conductance of the vacuum chamber as imposed by the design of small aperture magnets. The most stringent conditions are encountered in some of the experiments due to the required small beam pipes in the central detectors and due to the locally increased ion energy. Indeed, the strong focussing of the two beams at the interaction points increases the space charge and therefore the electric force on the ions such that the impact energy increases to several keV. Measured room temperature yields for the relevant range of impact energies range from about 1 to 8 molecules/ion [17] and depend critically on the cleanliness of the surface. Special methods of surface conditioning of the beam pipes by vacuum firing, Ar-glow discharge cleaning and by *in-situ* bakeout are under study.

7. BEAM-INDUCED ELECTRON MULTIPACTING

Beam induced multipacting [18], which can arise through oscillatory motion of a cloud of photoelectrons and low energy secondary electrons bouncing back and forth between opposite vacuum chamber walls during successive proton bunches, represent a potential problem for the machine [19]. The key parameters for this process are:

- bunch intensity and bunch spacing,
- synchrotron radiation intensity,
- photoelectric and secondary electron yields including the effect of the angle of incidence,
- energy distribution of secondary electrons,
- photon reflectivity,

beam screen shape and dimensions as well as external electric and magnetic fields.

The average value of energy transferred to electrons may be of the order of 200 eV. Under situations where the secondary electron yield exceeds unity, the electron cloud may then grow indefinitely and, as a consequence, provoke electron-stimulated gas desorption. A first criterion for the onset of multipacting is obtained from the necessary condition that the transit time of electrons from wall to wall must be equal or less than the time between the passage of successive bunches so that the electron cloud can move in synchronism with the beam

$$N_b = \frac{r_p^2}{r_e L_{bb}}. \quad (14)$$

Here r_p (m) is the beam pipe radius, L_{bb} is the distance between bunches and r_e the classical electron radius. In the LHC the determining parameters like the beam screen radius, the bunch intensity and the bunch spacing are such that the wall-to-wall multipacting condition is satisfied between about 1/4 to 1/3 of the nominal current [20].

The consequence for the machine operation can be an additional heat load due to the power deposited by the photo-electrons in the wall of the cold vacuum system, electron-stimulated gas desorption and finally coherent beam oscillations of the proton beam with the electron cloud leading to emittance growth and ultimately to beam loss. These effects have been studied extensively over the past years and it was concluded that an average heat load of 0.2 W/m should be included in the cryogenic budget. To reduce the electron cloud effect, one must find ways to reduce the production rate of photo-electrons and to achieve a low secondary electron yield at the internal surface of the vacuum chamber and of the beam screen [21].

A second important condition, which has to be satisfied, is that the energy transfer to the electrons is sufficiently large to obtain a secondary electron yield, which exceeds unity. Detailed numerical simulations for the nominal operating conditions have shown that in case of a secondary electron yield exceeding 1.3 to 1.4 the electron cloud could grow indefinitely until it finally saturates due to non-linear effects and space charge [22].

Secondary electron yield data for ‘technical’ Cu and Al surfaces measured on samples in the laboratory indicate that for both materials a unit yield is exceeded at an electron energy of less than 50 eV [23] and that the respective yield versus energy curves peak at 2.2 and 2.7 between 300 and 450 eV respectively. Therefore, to be safe against electron multipacting, it will be essential to provide a vacuum chamber surface with a lower secondary electron yield and primarily for this reason aluminium has been excluded as a material for beam pipes. Even for the more favourable materials like copper or stainless steel, it will be necessary to reduce their secondary electron yield below this critical value by *in-situ* conditioning, i.e. beam scrubbing, with synchrotron radiation.

8. MECHANICAL DESIGN ASPECTS

8.1 Beam screen

The beam screen is cooled by two longitudinal cooling tubes placed in the vertical plane above and below the beam where this is acceptable from the point of view of the required beam aperture. For mechanical and magnetic reasons, the screen must be made of a low-permeability stainless steel, approximately 1 mm thick. A detailed description of the required electric, magnetic and mechanical characteristics of the beam screen may be found in [23] and [24]. The inner wall, exposed to the electric field of the beam, is coated with a 0.05 mm layer of high-conductivity copper to keep the electric impedance low [25]. With this mechanical design an optimum compromise has to be found between many, partially conflicting requirements. For example, the good electric conductivity of the copper conflicts with the magnetic forces produced by eddy currents during a magnet quench. These forces have been evaluated at several tonnes per m and impose the mechanical strength of the screen. A list of main design parameters is given in Table 5.

Table 5
Beam screen design parameters

Aperture at 5 K radial/vertical	mm	45.5 / 35.7
Length	m	~16
Wall thickness	mm	~ 1
Material		Mn alloyed stainless steel
Magnetic permeability		< 1.005
Temperature	K	5 - 20
Cooling tubes (number/inner diameter)	mm	2 / 3.7
Cooling capacity	W/m	1
Impedance longitudinal transverse @ 3.3 kHz	Ohm	< 0.5 < 10 ¹⁰
Quench resistance @ $B \, dB/dt = 300 \, T^2s^{-1}$		> 50
Quench stress deformation	MPa mm	340 < 0.7
Copper coating @ RRR ~ 100	mm	0.05
Pumping slots (effective area)	%	2-4

8.1.1 Aperture

The cross section of the beam screen inserted in the magnet cold bore has been shown in Fig. 5. Since the space inside the cold bore is very limited, a design, which maximises the aperture available for the beam, must be found. The section is the result of an extensive study which takes into account the beam requirements at all stages of operation from injection, beam cleaning, colliding beams, to beam dumping. An individual beam screen for a dipole magnet is approximately 16-m long and its nominal clearance to the cold bore is less than 0.5 mm. It will be a technical challenge to meet these very tight dimensional tolerances and the required straightness.

The beam screens in one half-cell will be cooled in series by helium with 5 K inlet and 20 K outlet temperature. The preferred method for the attachment of the cooling tubes is by laser welding to minimise deformation and to keep the heat affected zone of the welds as small as possible. After the screen has been inserted in the magnet cold bore, there should remain a small annular gap to obtain on the one hand a good centring but on the other a low thermal contact.

8.1.2 Magnetic properties

The magnetic permeability of the beam screen and its components must be very low. Since any asymmetry in the distribution of magnetic material could give rise to undesirable harmonics of the magnetic guiding field of the beam. The specification imposes a magnetic permeability not exceeding 1.005 at the low temperature. This requirement eliminates more conventional types of stainless steels used in vacuum applications, e.g. 304 and 316 type steels, and imposes the use of highly stable austenitic stainless steels alloyed with Mn and N [26].

8.1.3 Copper coating and magnet quench

The inner surface of the screen must be coated with high-conductivity copper to obtain good electric conductivity. The thickness chosen for this copper layer results from an optimisation of several conflicting requirements:

A sufficiently thick, high conductivity layer will reduce the power dissipated by image currents, provide a low electric impedance and thus limit the growth rate for the transverse resistive-wall beam instability. A larger power dissipation would require more or larger helium cooling channels and thus complicate the design or reduce the vertical aperture. On the other hand, a thicker copper layer will entail larger eddy currents and electro-mechanical forces during a magnet quench and hence require a mechanically stronger, i.e. thicker beam screen, which again reduces the aperture. The compromise is 0.05 mm of copper and a ~ 1 -mm wall thickness for the stainless steel tube. The stresses induced in the beam screen during a magnet quench, results in a ~ 0.7 -mm deflection in the horizontal plane. Among the different methods for producing the copper layer roll-bonding of copper onto stainless steel strips is the most cost effective for a series production. The coated strip is then shaped into the final profile in a continuous tube-forming machine with a single longitudinal laser weld.

8.2 Beam screen interconnects

The mechanical design of the cold arc vacuum system requires a large number of interconnections for the beam vacuum between the beam screens of adjacent magnets. Following the proven design of the LEP-type RF-finger contacts a new concept has been developed which takes into account the large thermal contraction (approx. 45 mm) between room temperature and operating temperature [27]. An important design criterion to be met is the requirement of installation and alignment of the long cryomagnets without the risk of damaging the delicate finger contacts even in case of lateral offsets of up to 4 mm. The principle of the design is shown in Fig. 12. To by-pass the RF bellows, the beam screen cooling tubes are joined in the insulation vacuum enclosure by a flexible tubing. With this concept the risk of a helium leak affecting the critical beam vacuum can be minimised. In the final cold position the required smooth and well-defined electric contact is established with a controlled force of the RF contact fingers.

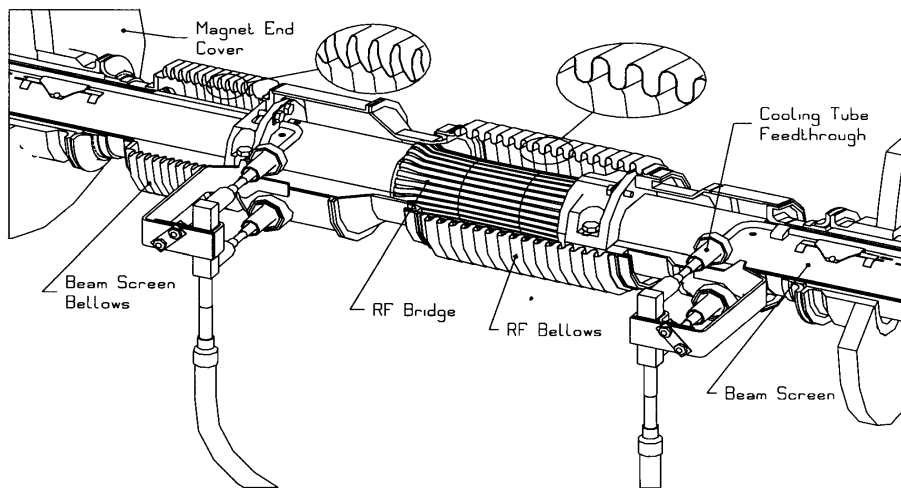


Fig. 12 Beam vacuum interconnect

9. SUMMARY

The design of the LHC vacuum system must satisfy a number of requirements, which depend not only on vacuum issues but also on considerations of both beam impedance and heat losses into the cryogenic system and/or the superconducting magnets. The pumping relies entirely on cryopumping of the 1.9 K cold bore surface, which offers a practically unlimited capacity for all gases except helium. The detailed design of the vacuum system is strongly influenced by the relatively large amount of synchrotron radiation, which represents a significant source of photon-stimulated outgassing, creates photoelectrons and is thus a driving mechanism for beam-induced multipacting. The beam induced heat load to the 1.9 K system has a large importance for the design and imposes by itself the presence of an actively-cooled beam screen. The intense proton bunches with their high peak

current lead to energetic ions which strike the walls and may cause ion-induced desorption and ion-induced pressure rise. Due to the cryogenic temperature of the walls, most molecular species are strongly cryosorbed and stick to the surface. This effect leads to a build-up of layers of cryosorbed gas, which in turn may desorb either thermally (vapour pressure effect) or by photon-stimulated desorption (re-cycling effect).

ACKNOWLEDGEMENTS

The description of the LHC vacuum system presented here reflects the work of many colleagues in the LHC Vacuum Group. The important contributions, in particular from the groups LHC-CRI, EST-SM and SL-AP are also gratefully acknowledged.

REFERENCES

- [1] The LHC Study Group, The Large Hadron Collider, Conceptual Design, CERN/AC/95-05 (1995).
- [2] L. Evans and Ph. Lebrun, Progress in Construction of the LHC, LHC Project Report 239 (1998).
- [3] J.C. Brunet, et al., LHC-Project Report 280 and PAC-99, New York, (1999).
- [4] A.G. Mathewson et al., EPAC-94, London, 1994.
- [5] A.G. Mathewson et al., PAC-95, Dallas, 1995.
- [6] O. Gröbner, Vacuum, 45, 767 (1995).
- [7] O. Gröbner, 10th Int. Conf. On High Energy Accelerators, Protvino, July 1977.
- [8] O. Gröbner, PAC-97, Vancouver 1997.
- [9] E. Wallén, J. Vac. Sci. Technol. A 15(2), march/April 1997.
- [10] V.V. Anashin, O.B. Malyshev, R. Calder and O. Gröbner, Vacuum 53, 269-272 (1999).
- [11] C. Benvenuti, R. Calder and G. Passardi, J. Vac. Sci. Technol. 13, 6, Nov/Dec. (1976).
- [12] R. Calder et al., J. Vac. Sci. Technol. A 14(4), Jul/Aug 1996.
- [13] P. Redhead et al., The Physical Basis of Ultrahigh Vacuum, AIP (1993).
- [14] O. Gröbner and R. Calder, IEEE Trans. Nucl. Sci., NS-20, 760, 1973.
- [15] F. Rieke and W. Prepejchal, Phys. Rev. A 6, 1507 (1972).
- [16] J.C. Barnard, I. Bojko and N. Hilleret, Vacuum 47, 4, 347 (1996).
- [17] I.R. Collins, O. Gröbner, P. Lepeule and R. Veness, EPAC-98, Stockholm (1998).
- [18] O. Gröbner, 10th Int. Conf. on High Energy Accelerators, Protvino, July 1977.
- [19] F. Zimmermann, LHC Project Report 95, 27 February 1997.
- [20] O. Gröbner, PAC-97, Vancouver, 1997.
- [21] V. Baglin, I.R. Collins and O. Gröbner, EPAC-98, Stockholm, 1998.
- [22] O. Brüning et al., PAC-99, New York (1999).
- [23] A. Poncet et al., EPAC-94, London, 1994.
- [24] P. Cruikshank et al., PAC-97, Vancouver, 1997.
- [25] F. Ruggiero, R. Caspers and M. Morvillo, PAC-97, Vancouver, 1997.
- [26] S. Sgobba and G. Hochoertler, International Congress Stainless Steel, to be published (1999).
- [27] R. Veness et al., PAC-99, New York (1999).